Role of ν-induced reactions on lead and iron in neutrino detectors

E. Kolbe[1,*] and K. Langanke[2]
[1]*Institut für Kernphysik I, Forschungszentrum Karlsruhe, Germany*
[2]*Institute for Physics and Astronomy, University of Aarhus, Aarhus, Denmark*
(Received 17 March 2000; revised manuscript received 26 October 2000; published 25 January 2001)

We have calculated cross sections and branching ratios for neutrino-induced reactions on ^{208}Pb and ^{56}Fe for various supernova and accelerator-relevant neutrino spectra. This was motivated by the facts that lead and iron will be used on the one hand as target materials in future neutrino detectors and, on the other hand, have been and are still used as shielding materials in accelerator-based experiments. In particular we study the inclusive ^{56}Fe$(\nu_e,e^-)^{56}$Co and ^{208}Pb$(\nu_e,e^-)^{208}$Bi cross sections and calculate the neutron energy spectra following the decay of the daughter nuclei. These reactions give a potential background signal in the KARMEN and LSND experiment and are discussed as a detection scheme for supernova neutrinos in the proposed OMNIS and LAND detectors. We also study the neutron emission following the neutrino-induced neutral-current excitation of ^{56}Fe and ^{208}Pb.

DOI: 10.1103/PhysRevC.63.025802 PACS number(s): 23.40.Bw, 13.10.+q, 25.30.Pt, 26.65.+t

I. INTRODUCTION

Neutrinos play a decisive role in many aspects of astrophysics and determining their properties is considered the most promising gateway to novel physics beyond the standard model of elementary particle physics. Thus detecting and studying accelerator-made or astrophysical neutrinos is a forefront research issue worldwide with many ongoing and planned activities.

One of the fundamental questions currently investigated is whether neutrinos have a finite mass. This question can be answered by the potential detection of neutrino oscillations which would establish the existence of at least one family of massive neutrinos. Furthermore, the existence of massive neutrinos might have profound consequences on many branches of cosmology and astrophysics, e.g., the expansion of the universe and the formation of galaxies, while neutrino oscillations can have interesting effects on supernova nucleosynthesis [1].

From the many experiments directly searching for neutrino oscillations, only the LSND Collaboration has reported positive candidate events [2]. Indirect evidence for neutrino oscillations arises from the deficit of solar neutrinos, as observed by all solar-neutrino detectors [3], and the suppression and its angular dependence of events induced by atmospheric ν_μ neutrinos in Superkamiokande [4,5]. As a result of the obvious importance, the oscillation results implied from these experiments will be cross checked by future long-base-line experiments like MINOS [6]. From the detectors currently operable KARMEN has a neutrino-oscillation sensitivity similar to the LSND experiment. Currently, the KARMEN Collaboration has not observed oscillations covering most of the oscillation parameter space for the positive LSND result [7].

A type II supernova releases most of its energy in terms of neutrinos. Supernova neutrinos from SN87a have been observed by the Kamiokande and IMB detectors [8,9] and have confirmed the general supernova picture. The observed events were most likely due to $\bar{\nu}_e$ antineutrinos. However, the models predict distinct differences in the neutrino distributions for the various families and thus a more restrictive test of the current supernova theory requires the abilities of neutrino spectroscopy by the neutrino detectors. Current (e.g., Superkamiokande and SNO) and future detectors (including the proposed OMNIS [10,11] and LAND [12] projects) have this capability and will be able to distinguish between the different neutrino types and determine their individual spectra. For the water Cerenkov detectors (SNO and Superkamiokande) ν_x neutrinos can be detected by specific neutral-current events [13,14], while the OMNIS and LAND detectors are proposed to detect neutrons spallated from target nuclei by charged- and neutral-current neutrino interactions.

Some of the supernova-neutrino or neutrino-oscillation detectors use iron or lead as detector material (e.g., MINOS, LAND, and OMNIS) or have adopted steel (LSND, KARMEN) and lead (LSND) shielding. Thus, precise theoretical estimates of the neutrino-induced cross sections on Fe and Pb are required for a reliable knowledge of the detection signal or the appropriate simulation of background events. We note that the KARMEN Collaboration has recently used its sensitivity to the ^{56}Fe$(\nu_e,e^-)^{56}$Co background events to determine a cross section for this reaction [15]. In Ref. [16] we have calculated this cross section in a hybrid model in which the allowed transitions have been studied based on the interacting shell model, while the forbidden transitions were calculated within the continuum random phase approximation. In this paper we extend this investigation and study the charged- and neutral-current reactions on ^{56}Fe and ^{208}Pb for various accelerator-based and supernova neutrino distributions. In particular, we determine the ^{208}Pb(ν_e,e^-) cross sections for the LSND neutrino spectra which will serve for even improved background simulations for this detector. Our calculations of supernova neutrino reaction cross sections on ^{56}Fe and ^{208}Pb are aimed to guide the design of supernova

*Permanent address: Departement für Physik und Astronomie der Universität Basel, Basel, Switzerland.

neutrino detectors like OMNIS and LAND. With this goal in mind we have calculated the energy spectrum of neutrons knocked out by the charged-current or neutral-current neutrino-induced excitation of ^{56}Fe and ^{208}Pb. To allow also the exploration of potential oscillation scenarios we have calculated the cross sections and neutron spectra for various supernova neutrino spectra.

II. THEORETICAL MODEL

Besides the total cross sections, the partial cross sections for neutrino-induced particle knockout are of relevance to estimate the signal and background of the various detectors. We will calculate these partial cross sections in a two-step process (e.g., for the charged-current reaction)

$$\underbrace{\nu + {}_{Z}X_{N} \rightarrow l + {}_{Z+1}X^{*}_{N-1}}_{1.\ \text{RPA}} \Rightarrow \underbrace{{}_{Z+1}X^{*}_{N-1} \rightarrow \begin{cases} {}_{Z+1}X_{N-2} + n \\ {}_{Z}X_{N-1} + p \\ {}_{Z-1}X_{N-3} + \alpha \\ {}_{Z+1}X_{N-1} + \gamma \end{cases}}_{2.\ \text{Statistical Model}}$$

In the first step, we calculate the ν-induced spectrum $(d\sigma/d\omega)(\omega)$ in the daughter nucleus at excitation energy ω. We consider multipole excitations of both parities and angular momenta $\lambda \leqslant 9$, using the formalism developed in [17]. These multipole operators, denoted by λ^{π}, depend on the momentum transfer q.

Our strategy to calculate $(d\sigma/d\omega)(\omega)$ has been different for ^{56}Fe and ^{208}Pb. For ^{56}Fe we adopt the same hybrid model which has already been successfully applied in [16]. That is, we calculate all nuclear responses within the random phase approximation (RPA). However, the RPA does not usually recover sufficient nucleon-nucleon correlations to reliably reproduce the quenching and fragmentation of the Gamow-Teller (GT) strength distribution in nuclei. For this reason we determine the response of the $\lambda^{\pi}=1^{+}$ operator on the basis of an interacting shell-model calculation performed within the complete pf shell. Such a study has been proven to reproduce the experimental GT_{-} (in which a neutron is changed into a proton) and GT_{+} (in which a proton is changed into a neutron) distributions on ^{56}Fe well [18], if the response is quenched by a universal factor $(0.74)^2$ [19–21]. However, the GT operator corresponds to the appropriate $\lambda^{\pi}=1^{+}$ operator only in the limit of momentum transfer $q \rightarrow 0$. As has been pointed out in [16,22], consideration of the finite-momentum transfer in the operator results in a reduction of the cross sections, caused by the destructive interference with the higher-order operator $\tau \vec{\sigma} \vec{r} \cdot \vec{p}$. To account for the effect of the finite-momentum transfer we have performed RPA calculations for the $\lambda^{\pi}=1^{+}$ multipole operator at finite-momentum transfer q [i.e., $\lambda(q)$] and for $q=0$ [i.e., $\lambda(q=0)$] and have scaled the shell-model GT strength distribution by the ratio of $\lambda(q)$ and $\lambda(q=0)$ RPA cross sections. The correction is rather small for ν_e neutrinos stemming from muon-decay-at-rest (i.e., for LSND and KARMEN) or for supernova ν_e neutrinos. The correction is, however, sizable if neutrino oscillations occur in the accelerator-based experiments or a supernova [22].

For ^{208}Pb a converged shell-model calculation of the GT strength distribution is yet not computationally feasible. Thus we have also calculated the $\lambda^{\pi}=1^{+}$ response within the RPA approach. Note that our RPA approach fulfills the Fermi and Ikeda sum rules. As the S_{β^+} strength (in this direction a proton is changed into a neutron) is strongly suppressed for ^{208}Pb, the Ikeda sum rule fixes the S_{β^-} strength. We have renormalized the $\lambda^{\pi}=1^{+}$ strength in ^{208}Pb by the universal quenching factor which, due to a very slight A dependence, is recommended to be $(0.7)^2$ in ^{208}Pb [21]. Thus the Ikeda sum rule reads $S_{\beta_-} - S_{\beta_+} \approx S_{\beta_-} = 3 \times (0.7)^2 \times (N-Z)$. For the other multipole operators no experimental evidence exists for such a rescaling and we have used the RPA response.

In our RPA calculations we have chosen the single-particle energies from an appropriate Woods-Saxon potential, which has been adjusted to reproduce the relevant particle thresholds. As residual interaction we used the zero-range Landau-Migdal force from [23]. However, it is well known that this parametrization places the isobaric analog state (IAS) in ^{208}Bi at too high an energy. This is cured by changing the parameter, which multiplies the $\tau_i \cdot \tau_j$ term in the interaction from $f_0' = 1.5$ to the value 0.9 [24]. After this adjustment the IAS is very close ($E_{IAS} = 15.4$ MeV) to the experimental position (15.16 MeV). Furthermore, our RPA parametrization has been demonstrated to describe the ^{208}Pb(p,n) reaction data at small forward angle well [24]. Our RPA approaches are described in detail in Refs. [25,26]. We note that this approach gives quite satisfying results for neutrino scattering [25,27,28], muon capture [29], and electron scattering [30].

After having determined the neutrino-induced excitation spectrum in the daughter nucleus, we calculate in the second step for each final state with well-defined energy, angular momentum, and parity the branching ratios into the various decay channels using the statistical model code SMOKER [31]. The decay channels considered are proton, neutron, α, and γ emission. As possible final states in the residual nucleus the SMOKER code considers the experimentally known levels supplemented at higher energies by an appropriate level density formula. Note that the SMOKER code has been successfully applied to many astrophysical problems and that we empirically found good agreement between p/n branching ratios calculated with SMOKER and within the continuum RPA for several neutral-current reactions on light nuclei [25].

As supernova and accelerator-produced neutrinos have an energy spectrum, the final results (total and partial cross sections) are obtained by folding with the appropriate neutrino spectra.

III. RESULTS

A. Reactions induced by decay-at-rest neutrinos

The ν_e neutrinos produced in the muon decay-at-rest (DAR) have the characteristic Michel energy spectrum

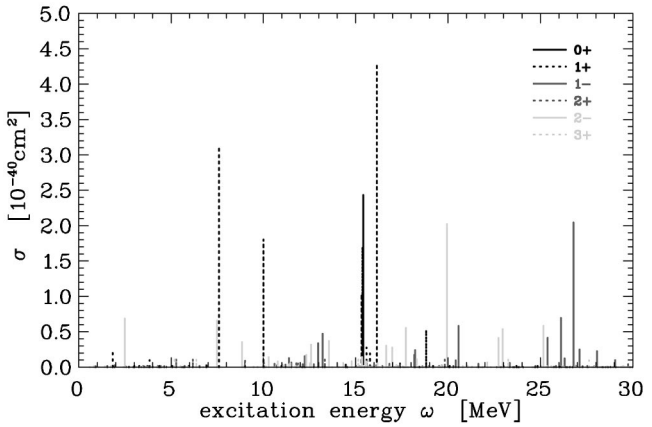

FIG. 1. Multipole decomposition of the RPA response for the charged-current (ν_e, e^-) reaction on ^{208}Pb induced by DAR ν_e neutrinos.

$$n(E_\nu) = \frac{96E_\nu^2}{M_\mu^4}(M_\mu - 2E_\nu), \tag{1}$$

where M_μ is the muon mass and E_ν the neutrino energy.

Our calculated excitation spectrum for the ^{56}Fe$(\nu_e, e^-)^{56}$Co reaction is shown in [16]. Figure 1 shows the RPA response for the ^{208}Pb$(\nu_e, e^-)^{208}$Bi reaction, calculated for a muon decay-at-rest neutrino spectrum. The collective GT transition is found at an excitation energy of around $E_x = 16$ MeV in ^{208}Bi, again close to the centroid of the experimentally observed GT strength distribution which is at around 15.6 MeV [32,33]. As has already been observed in [34], RPA calculations also predict GT$_-$ strength at lower excitation energies, which then correspond mainly to individual single-particle transitions. As a result of phase space, these low-lying transitions are noticeably enhanced in neutrino-induced reactions with respect to the collective transition. Our calculation indicates the low-lying GT strength to be mainly centered at around $E_x = 7.5$ MeV in ^{208}Bi. There might be some evidence for such a transition in the experimental (p,n) spectra on ^{208}Pb [32]. However, a doubtless experimental confirmation would be quite desirable. The first-forbidden transitions lead mainly to 1^- and 2^- states in ^{208}Bi. In our calculation these transitions are fragmented over states in the energy interval between 17 MeV and 26 MeV, although we find 2^- strength also at rather low excitation energies $E_x = 2.5$ MeV and 7.5 MeV. Experimentally 2^- strength has been observed at $E_x = 2.8$ MeV [32].

To check the reliability of our approach we have performed several additional calculations. At first we have calculated the GT response for ^{56}Fe within the RPA approach. Then the GT distribution is focused on two strong transitions at $E_x = 2$ MeV and 10.5 MeV in ^{56}Co, corresponding to the change of a $f_{7/2}$ neutron into $f_{7/2}$ and $f_{5/2}$ protons, respectively, clearly showing the inappropriate fragmentation of the GT strength within the RPA. However, we find that this shortcoming does not strongly influence the calculated cross section. If we correct for the overestimation of the total RPA S_{β_-} strength compared with the shell model (and data), we find an RPA GT contribution to the ^{56}Fe$(\nu_e, e^-)^{56}$Co cross section in close agreement to the shell model result (better than 3%). We thus conclude that our total ^{208}Pb$(\nu_e, e^-)^{208}$Bi cross section, for which we could not calculate the $\lambda^\pi = 1^+$ contribution on the basis of the shell model, is probably quite reliable.

TABLE I. Total cross sections for charged-current neutrino scattering on nuclei for electron neutrinos from pion-decay-at-rest. The cross sections are given in units of 10^{-42} cm^2; exponents are given in parentheses.

Neutrino reaction	Cross section
^{56}Fe$(\nu_e, e^-\gamma)^{56}$Co	1.25 (2)
^{56}Fe$(\nu_e, e^- n)^{55}$Co	3.33 (1)
^{56}Fe$(\nu_e, e^- p)^{55}$Fe	7.83 (1)
^{56}Fe$(\nu_e, e^- \alpha)^{52}$Mn	3.52 (0)
^{56}Fe$(\nu_e, e^-)X$	2.40 (2)
^{208}Pb$(\nu_e, e^-\gamma)^{208}$Bi	3.24 (2)
^{208}Pb$(\nu_e, e^- n)^{207}$Bi	3.29 (3)
^{208}Pb$(\nu_e, e^- p)^{207}$Pb	4.77 (−1)
^{208}Pb$(\nu_e, e^- \alpha)^{204}$Tl	1.01 (0)
^{208}Pb$(\nu_e, e^-)X$	3.62 (3)

As a result of the energy and momentum transfer involved, muon capture is mainly sensitive to forbidden transitions ($\lambda^\pi = 1^-$ and 2^- for ^{56}Fe and $\lambda^\pi = 1^+$, 2^+, and 3^+ for ^{208}Pb). We have tested our model description for forbidden transitions by calculating the total muon capture rates for ^{56}Fe and ^{208}Pb and obtain results (4.46×10^6 s^{-1} and 16.1×10^6 s^{-1}) which agree rather well with experiment [$(4.4\pm0.1)\times10^6$ s^{-1} and $(13.5\pm0.2)\times10^6$ s^{-1}, respectively [35]]. Further details on these studies will be published elsewhere [36].

The KARMEN Collaboration has measured the total ^{56}Fe$(\nu_e, e^-)^{56}$Co cross section for the DAR neutrino spectrum and obtains $\sigma = (2.56\pm1.08\pm0.43)\times10^{-40}$ cm^2 [15]. We calculate a result in close agreement, $\sigma = 2.4\times10^{-40}$ cm^2. In Table I we have listed the partial cross sections into the various decay channels. As the IAS at $E_x = 3.5$ MeV and most of the GT$_-$ strength resides below the particle thresholds in ^{56}Co (the proton and neutron thresholds are at 5.85 MeV and 10.08 MeV, respectively), most of the neutrino-induced reactions on ^{56}Fe leads to particle-bound states, which then decay by γ emission. Because of the lower threshold, neutrino-induced excitation of particle-unbound states in ^{56}Co is dominantly followed by proton decays. The rather high threshold energy (7.76 MeV) and the larger Coulomb barrier makes decay into the α channel rather unimportant.

Now we turn our discussion to ^{208}Pb which is the shielding material of the LSND detector. The simple $(N-Z)$ scaling of the Fermi and Ikeda sum rules indicates that the (ν, e^-) cross section on ^{208}Pb is significantly larger than on ^{56}Fe. The cross section is additionally enlarged by the strong Z dependence of the Fermi function. In total we find that the (ν_e, e^-) cross section on ^{208}Pb is about 15 times bigger than for ^{56}Fe. Furthermore, as the IAS energy and the GT$_-$

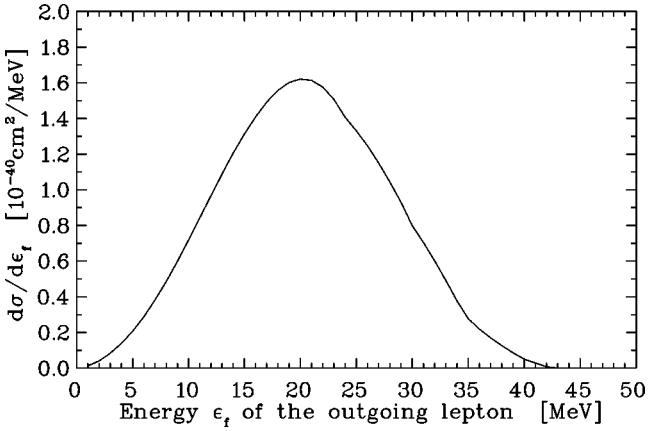

FIG. 2. The ^{208}Pb$(\nu_e,e^-n)^{207}$Bi cross section for DAR neutrinos as function of final electron energy.

strength are above the neutron threshold in ^{208}Bi at 6.9 MeV, most of the (ν_e,e^-) cross section leads to particle-unbound states. These expectations are borne out by a detailed calculation which finds a total cross section of 3.62×10^{-39} cm^2. The partial ^{208}Pb$(\nu_e,e^-n)^{207}$Bi cross section dominates and amounts to about 91% of the total cross section. As can be seen in Table I, the remaining cross section mainly goes to particle-bound levels and hence decays by γ emission.

For the general reasons given above, our theoretical estimate for the ^{208}Pb$(\nu_e,e^-)^{208}$Bi cross section is probably quite reliable and should be useful for improved background simulations of the LSND detector. It is also quite interesting to turn the problem around and ask whether the LSND Collaboration can actually measure this cross section. To this end we have estimated the total number of neutrino-induced events in the lead shielding [37] (volume $V=20$ m^3, density $\rho=11.3$ g/cm^3) of the LSND detector assuming an annual LSND neutrino flux of 3×10^{13}/yr. Then our ^{208}Pb$(\nu,e^-)^{208}$Bi cross section translates into 200 000 events for the 3 yr running time from 1996 to 1998. In about 180 000 events a neutron is knocked out of the lead target. The electron will not travel directly into the detector, but will shower in the shielding producing photons which in turn might reach the detector in which they produce Compton electrons. The KARMEN Collaboration has observed this process for the ^{56}Fe shielding and quotes an efficiency of their detector of 0.44%. If the LSND detector has a comparable efficiency for this process, it should be able to observe the ^{208}Pb$(\nu_e,e^-n)^{207}$Bi cross section where the events are most likely at the edges. On the other hand, the correlated observation of a neutron and a lepton constitutes the LSND neutrino oscillation signal. For this reason, the LSND Collaboration suppresses the events stemming from neutrino interactions on lead by appropriate energy and spatial cuts. However, our calculated ^{208}Pb(ν_e,e^-n) cross section might allow the LSND Collaboration to further improve their background simulations.

The LSND oscillation experiment studies their events as a function of energy of the outgoing lepton, setting cuts at 20 MeV, 36 MeV, and 53 MeV. We have therefore also calculated the ^{208}Pb$(\nu,e^-n)^{207}$Bi cross section as function of the final lepton energy, which is shown in Fig. 2.

TABLE II. Total cross sections for charged-current neutrino scattering on nuclei for muon neutrinos with the LSND pion-decay-in-flight spectrum. The cross sections are given in units of 10^{-42} cm^2; exponents are given in parentheses.

Neutrino reaction	Cross section
^{56}Fe$(\nu_\mu,\mu^-\gamma)^{56}$Co	2.24 (2)
^{56}Fe$(\nu_\mu,\mu^-n)^{55}$Co	6.62 (2)
^{56}Fe$(\nu_\mu,\mu^-p)^{55}$Fe	1.33 (3)
^{56}Fe$(\nu_\mu,\mu^-\alpha)^{52}$Mn	2.23 (2)
^{56}Fe$(\nu_\mu,\mu^-)X$	2.44 (3)
^{208}Pb$(\nu_\mu,\mu^-\gamma)^{208}$Bi	1.23 (3)
^{208}Pb$(\nu_\mu,\mu^-n)^{207}$Bi	1.02 (4)
^{208}Pb$(\nu_\mu,\mu^-p)^{207}$Pb	2.89 (0)
^{208}Pb$(\nu_\mu,\mu^-\alpha)^{204}$Tl	3.31 (1)
^{208}Pb$(\nu_\mu,\mu^-)X$	1.15 (4)

The LSND neutrino beam has a small admixture of ν_μ neutrinos stemming from pion-in-flight (DIF) decays. These neutrinos have in fact high enough energies to significantly produce muons by the charged-current (ν_μ,μ^-) reaction [this beam property allowed the LSND Collaboration to measure the inclusive ^{12}C$(\nu_\mu,\mu^-)^{12}$N cross section and to test universality in a neutrino experiment on nuclei [38]]. For the oscillation search events stemming from the (ν_μ,μ^-n) reaction, with a possible misinterpretation of the lepton in the final channel, are considered a possible background. For this reason we have also calculated the total and partial (ν_μ,μ^-) cross sections on ^{208}Pb for the LSND DIF ν_μ neutrino spectrum. The results are shown in Table II.

We note that the ''most effective'' neutrino energy defined by

$$\overline{E}_\nu=\frac{\int E_\nu\sigma(E_\nu)dE_\nu}{\int\sigma(E_\nu)dE_\nu} \tag{2}$$

is larger for DIF neutrinos ($\overline{E}_\nu=170$ MeV) than for DAR neutrinos ($\overline{E}_\nu=37$ MeV). Thus, even if the mass difference between muon and electron is considered, the phase space favors the reaction induced by DIF ν_μ neutrinos. Consequently the total cross section for the charged-current reaction on ^{208}Pb induced by DIF ν_μ neutrinos is larger (by roughly a factor of 3) than induced by DAR ν_e neutrinos. Although the average excitation energy in the daughter nucleus is also slightly higher for DIF ν_μ neutrinos than for DAR ν_e neutrinos, the decay of the particle-unbound states is still dominantly into the neutron channel.

The LSND Collaboration observes candidate events which might imply $\nu_\mu\rightarrow\nu_e$ neutrino oscillations [39]. If this is the case, the DIF ν_μ neutrinos can have changed into ν_e neutrinos before reaching the detector, now allowing for ^{208}Pb(ν_e,e^-) reactions triggered by ν_e neutrinos with a sig-

TABLE III. Total cross sections for charged-current (ν_e, e^-) neutrino scattering on ^{56}Fe and ^{208}Pb nuclei for electron neutrinos with the LSND pion-decay-in-flight neutrino spectrum. The cross sections are given in units of 10^{-42} cm^2; exponents are given in parentheses.

Neutrino reaction	Cross section
$^{56}\mathrm{Fe}(\nu_e, e^- \gamma)\,^{56}\mathrm{Co}$	5.80 (2)
$^{56}\mathrm{Fe}(\nu_e, e^- n)\,^{55}\mathrm{Co}$	1.91 (3)
$^{56}\mathrm{Fe}(\nu_e, e^- p)\,^{55}\mathrm{Fe}$	3.84 (3)
$^{56}\mathrm{Fe}(\nu_e, e^- \alpha)\,^{52}\mathrm{Mn}$	6.48 (2)
$^{56}\mathrm{Fe}(\nu_e, e^-)X$	6.98 (3)
$^{208}\mathrm{Pb}(\nu_e, e^- \gamma)\,^{208}\mathrm{Bi}$	2.75 (3)
$^{208}\mathrm{Pb}(\nu_e, e^- n)\,^{207}\mathrm{Bi}$	3.49 (4)
$^{208}\mathrm{Pb}(\nu_e, e^- p)\,^{207}\mathrm{Pb}$	1.00 (1)
$^{208}\mathrm{Pb}(\nu_e, e^- \alpha)\,^{204}\mathrm{Tl}$	1.12 (2)
$^{208}\mathrm{Pb}(\nu_e, e^-)X$	3.78 (4)

nificantly higher energy. We have studied the respective cross sections and have summarized them in Table III.

For completeness, Tables II and III also list the (ν_μ, μ^-) and (ν_e, e^-) cross sections on ^{56}Fe, in both cases calculated for a DIF neutrino spectrum.

B. Supernova neutrinos

The observation of the neutrinos from SN1987a by the water Čerenkov detectors is generally considered as strong support that the identification of type II supernovas as core collapse supernovas is correct. Theoretical models predict that the protoneutron star formed in the center of the supernova cools by the production of neutrino pairs, where the luminosity is approximately the same for all three neutrino families. The interaction of the neutrinos with the dense surrounding, consisting of ordinary neutron-rich matter, introduces characteristic differences in the neutrino distributions for the various families. As the μ and τ neutrinos and their antiparticles (combined referred to as ν_x) have not enough energy to generate a muon or τ lepton, they decouple deepest in the star, i.e., at the highest temperature, and have an average energy of $\overline{E_\nu}=25$ MeV. As the ν_e and $\overline{\nu_e}$ neutrinos interact with the neutron-rich matter via $\nu_e + n \rightarrow p + e^-$ and $\overline{\nu_e} + p \rightarrow n + e^+$, the $\overline{\nu_e}$ neutrinos have a higher average energy ($\overline{E_\nu}=16$ MeV) than the ν_e neutrinos ($\overline{E_\nu}=11$ MeV). Clearly an observational verification of this temperature hierarchy would establish a strong test of our current supernova models.

The distribution of the various supernova neutrino species is usually described by a Fermi-Dirac spectrum

$$n(E_\nu) = \frac{1}{F_2(\alpha) T^3} \frac{E_\nu^2}{\exp[(E_\nu/T) - \alpha] + 1}, \qquad (3)$$

where T, α are parameters fitted to numerical spectra, and $F_2(\alpha)$ normalizes the spectrum to unit flux. The transport calculations of Janka and Hillebrandt [40] yield spectra with

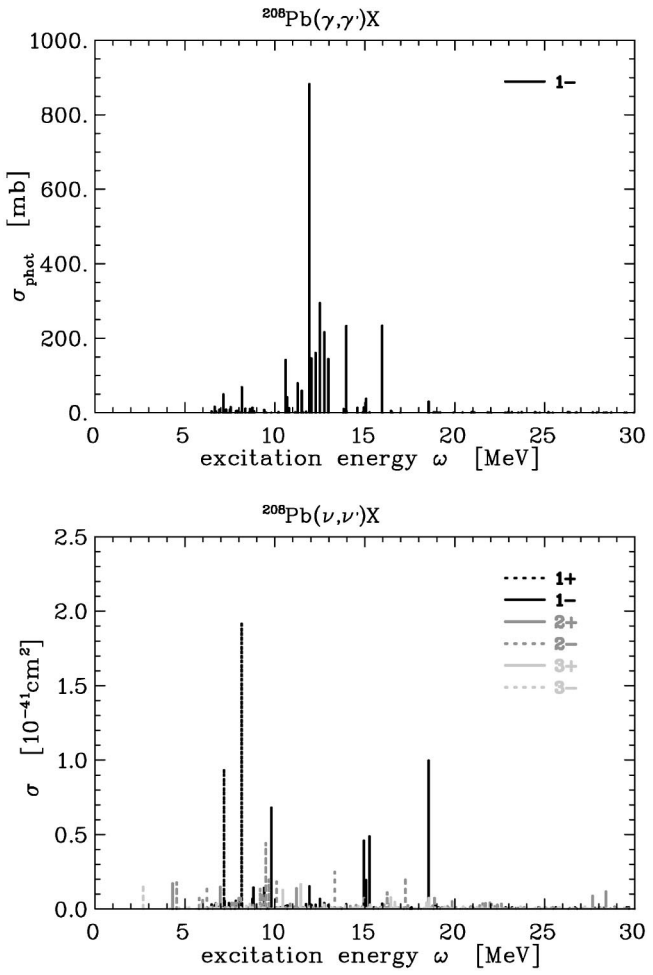

FIG. 3. Excitation spectrum of the ^{208}Pb nucleus for photoabsorption (upper part) in comparison to the spectrum excited by neutral current neutrino scattering (lower part), which is decomposed into the dominant multipole contributions.

$\alpha \sim 3$ for all neutrino species. While this choice also gives good fits to the ν_e and $\overline{\nu_e}$ spectra calculated by Wilson [41], their ν_x spectra favor $\alpha = 0$. In the following we will present results for charged- and neutral-current reactions on ^{56}Fe and ^{208}Pb for both values of α. In particular we will include results for those (T, α) values which are currently favored for the various neutrino types (T in MeV): $(T, \alpha) = (4,0)$ and (3,3) for ν_e neutrinos, (5,0) and (4,3) for $\overline{\nu_e}$ neutrinos, and (8,0) and (6.26,3) for ν_x neutrinos.

Before discussing our neutral-current results for ^{208}Pb we would like to present the multipole response as calculated within our RPA study. This is done in Fig. 3 which shows the ^{208}Pb photoabsorption cross section in the upper part as well as the excitation function for inelastic scattering on ^{208}Pb by neutrinos with a Fermi-Dirac distribution with parameters $T = 8$ MeV and $\alpha = 0$ in the lower part. The calculated photoabsorption cross section is fragmented between 10 and 16 MeV excitation energy centered around ~ 13 MeV. This is reasonably close to the experimental spectrum which is centered around 13.8 MeV with a width of 3.8 MeV [42]. Summing over all excitation energies we obtain 3.0

TABLE IV. Total cross sections for neutral-current neutrino scattering on nuclei for different neutrino energy spectra represented as Fermi-Dirac distributions. The cross sections are given in units of 10^{-42} cm^2 and are averaged over neutrinos and antineutrinos.

(T,α)	(4,0)	(6,0)	(8,0)	(10,0)	(3,3)	(4,3)	(6.26,3)
^{56}Fe$(\nu,\nu'\gamma)^{56}$Fe	2.9(0)	9.3(0)	1.9(1)	3.0(1)	1.9(0)	5.0(0)	1.7(1)
^{56}Fe$(\nu,\nu'n)^{55}$Fe	7.1(−1)	5.9(0)	2.1(1)	4.9(1)	2.3(−1)	1.3(0)	1.3(1)
^{56}Fe$(\nu,\nu'p)^{55}$Mn	5.6(−2)	6.8(−1)	3.1(0)	8.7(0)	1.3(−2)	1.1(−1)	1.6(0)
^{56}Fe$(\nu,\nu'\alpha)^{52}$Cr	9.4(−3)	1.2(−1)	5.5(−1)	1.6(0)	2.1(−3)	1.8(−2)	2.8(−1)
^{56}Fe$(\nu,\nu')X$	3.7(0)	1.6(1)	4.3(1)	9.0(1)	2.1(0)	6.4(0)	3.2(1)
^{208}Pb$(\nu,\nu'\gamma)^{208}$Pb	3.6(0)	1.2(1)	2.7(1)	4.8(1)	2.4(0)	6.1(0)	2.2(1)
^{208}Pb$(\nu,\nu'n)^{207}$Pb	1.1(1)	5.0(1)	1.4(2)	2.8(2)	5.8(0)	1.9(1)	1.0(2)
^{208}Pb$(\nu,\nu'p)^{207}$Tl	2.3(−5)	5.3(−4)	3.8(−3)	1.5(−2)	4.0(−6)	4.4(−5)	1.4(−3)
^{208}Pb$(\nu,\nu'\alpha)^{204}$Hg	1.2(−4)	4.7(−3)	4.7(−2)	2.3(−1)	1.2(−5)	2.2(−4)	1.3(−2)
^{208}Pb$(\nu,\nu')X$	1.4(1)	6.2(1)	1.6(2)	3.3(2)	8.1(0)	2.5(1)	1.2(2)

MeV b for the total photoabsorption cross section, which is in agreement with the classical Thomas-Reiche-Kuhn sum rule value (2.98 MeV b) and also lies within the range of experimental values (2.9−4.1 MeV b; see Table 5 of Ref. [43]).

The lower part of Fig. 3 demonstrates clearly that inelastic neutrino scattering additionally excites the spin response which is responsible for the two strong $J=1^-$ transitions around 10 MeV and 18 MeV. As expected from the general effects of the residual interaction the 2^- part of the spin dipole excitations is located a few MeV lower in energy than the 1^- strength [44]. We finally note that the Gamow-Teller strength is calculated between 7 MeV and 8 MeV, in close agreement with the experimentally observed $M1$ strength.

Table IV summarizes the total and partial cross sections for neutral current reactions on ^{56}Fe and ^{208}Pb. For ^{56}Fe the neutron and proton thresholds open at 11.2 MeV and 10.18 MeV, respectively. But despite the slightly higher threshold energy, the additional Coulomb barrier in the proton channel makes the neutron channel the dominating decay mode. With increasing average neutrino energies the total cross section grows. But this increase is noticeably weaker than for the nuclei ^{12}C and ^{16}O. This is related to the isovector dominance of the neutrino-induced reactions. In the $T=0$ nuclei ^{12}C and ^{16}O inelastic neutrino scattering has to overcome a rather large threshold to reach the $T=1$ excitation spectrum in the nuclei making the cross section rather sensitive to the neutrino spectrum.

The total and partial cross sections for charged current (ν_e,e^-) and $(\bar{\nu}_e,e^+)$ reactions on ^{56}Fe and ^{208}Pb are listed in Table V. As the average energy for supernova ν_e neutrinos ($\bar{E}_\nu \approx 11$ MeV) is less than for DAR neutrinos ($\bar{E}_\nu \approx 37$ MeV), the total cross sections are significantly smaller for supernova [i.e., $(T,\alpha)=(4,0)$ or $(3,3)$] neutrinos. Relatedly the low-energy excitation spectrum is stronger weighted by phase space. Hence, the ν_e-induced reaction on ^{56}Fe leads dominantly to particle-bound states ($\sim 60\%$) and therefore decays by γ emission. As for DAR neutrinos, the strongest decay mode for ν_e-induced reactions on ^{208}Pb is given by the neutron channel.

As lead is discussed as material for potential supernova neutrino detectors (such as LAND and OMNIS), the relevant neutrino-induced reactions on ^{208}Pb have been estimated previously. The first work, performed in [12], has been criticized and improved in [46]. These authors estimated the allowed transitions to the charged-current and neutral-current cross sections empirically using data from (p,n) scattering and from the $M1$ response to fix the Gamow-Teller contributions to the cross section. We note that these data place the GT$_-$ strength in one resonance centered just above the $2n$ threshold. Low-lying GT$_-$ transitions, as indicated by the present RPA calculation, have not been considered in [46]. Reference [46] completed their cross section estimates by calculating the first-forbidden contributions on the basis of the Goldhaber-Teller model.

Although the total charged-current ^{208}Pb$(\nu_e,e^-)^{208}$Bi cross section is strongly constrained by sum rules and our calculation and the work of Ref. [46] reproduce the energies of the IAS state and the main GT resonance, our results clearly deviate with increasing neutrino energies from the calculation of Ref. [46]. For ν_e neutrinos with a $(T,\alpha)=(3,3)$ Fermi-Dirac distribution our cross section (1.6×10^{-40} cm^2) is in rough agreement with the one obtained in [46]. [As [46] does not give the cross section for a $(T=3,\alpha=3)$ spectrum, we have estimated it from the cross sections given at neighboring temperatures taken from Table I of [46].] But with increasing neutrino energies our calculated cross sections become significantly smaller than the estimate given in [46], and for a ν_e spectrum with $(T,\alpha)=(8,0)$ our value (25×10^{-40} cm^2) is about 55% smaller than the estimate by Ref. [46] (58×10^{-40} cm^2). For the latter neutrino spectrum the cross section is dominated by forbidden transitions, and the observed difference might reflect the uncertainties of the Goldhaber-Teller model to describe this response.

For the total neutral-current cross sections on ^{208}Pb the estimates in [46] are noticeably larger than our results (by factors in the range of 2–3 for the various Fermi-Dirac spectra) for all energies. As pointed out by Woosley *et al.* [47] the total (ν,ν') cross sections on nuclei induced by super-

TABLE V. Total cross sections for charged-current neutrino scattering on nuclei for different neutrino energy spectra represented as Fermi-Dirac distributions. The cross sections are given in units of 10^{-42} cm^2.

(T,α)	(4,0)	(6,0)	(8,0)	(10,0)	(3,3)	(4,3)	(6.26,3)
^{56}Fe$(\nu_e,e^-\gamma)^{56}$Co	9.8(0)	3.2(1)	6.4(1)	1.0(2)	6.5(0)	1.7(1)	5.9(1)
^{56}Fe$(\nu_e,e^-n)^{55}$Co	7.5(−1)	8.2(0)	3.3(1)	8.1(1)	1.9(−1)	1.5(0)	2.0(1)
^{56}Fe$(\nu_e,e^-p)^{55}$Fe	5.4(0)	3.3(1)	1.0(2)	2.2(2)	2.2(0)	1.0(1)	7.3(1)
^{56}Fe$(\nu_e,e^-\alpha)^{52}$Mn	6.1(−2)	9.8(−1)	4.9(0)	1.4(1)	9.9(−3)	1.2(−1)	2.5(0)
^{56}Fe$(\nu_e,e^-)X$	1.6(1)	7.4(1)	2.0(2)	4.1(2)	8.9(0)	2.9(1)	1.5(2)
^{208}Pb$(\nu_e,e^-\gamma)^{208}$Bi	4.7(1)	1.3(2)	2.5(2)	4.0(2)	3.5(1)	7.6(1)	2.2(2)
^{208}Pb$(\nu_e,e^-n)^{207}$Bi	2.3(2)	9.9(2)	2.3(3)	4.0(3)	1.2(2)	4.2(2)	1.9(3)
^{208}Pb$(\nu_e,e^-p)^{207}$Pb	1.8(−2)	1.1(−1)	3.3(−1)	6.9(−1)	7.2(−3)	3.3(−2)	2.3(−1)
^{208}Pb$(\nu_e,e^-\alpha)^{204}$Tl	2.1(−2)	2.6(−1)	1.1(0)	3.0(0)	4.7(−3)	4.1(−2)	6.0(−1)
^{208}Pb$(\nu_e,e^-)X$	2.8(2)	1.1(3)	2.5(3)	4.5(3)	1.6(2)	4.9(2)	2.1(3)
^{56}Fe$(\nu_e,e^+\gamma^{56}$Mn	3.4(0)	1.1(1)	2.2(1)	3.6(1)	2.3(0)	5.7(0)	1.9(1)
^{56}Fe$(\overline{\nu_e},e^+n)^{55}$Mn	5.0(−1)	4.5(0)	1.7(1)	4.2(1)	1.5(−1)	9.4(−1)	1.0(1)
^{56}Fe$(\overline{\nu_e},e^+p)^{55}$Cr	4.3(−3)	5.5(−2)	2.7(−1)	8.4(−1)	9.3(−4)	8.1(−3)	1.3(−1)
^{56}Fe$(\overline{\nu_e},e^+\alpha)^{52}$V	6.7(−4)	1.1(−2)	6.7(−2)	2.3(−1)	1.2(−4)	1.3(−3)	2.8(−2)
^{56}Fe$(\overline{\nu_e},e^+)X$	3.9(0)	1.5(1)	3.9(1)	7.9(1)	2.4(0)	6.6(0)	2.9(1)
^{208}Pb$(\overline{\nu_e},e^+\gamma)^{208}$Tl	5.8(−1)	3.0(0)	7.9(0)	1.5(1)	2.7(−1)	1.1(0)	6.1(0)
^{208}Pb$(\nu_e,e^+n^{207}$Tl	4.9(−1)	3.8(0)	1.5(1)	3.9(1)	2.0(−1)	8.9(−1)	8.5(0)
^{208}Pb$(\overline{\nu_e},e^+p)^{207}$Hg	1.7(−7)	1.4(−5)	2.2(−4)	1.5(−3)	8.4(−9)	3.2(−7)	4.2(−5)
^{208}Pb$(\overline{\nu_e},e^+\alpha)^{204}$Au	4.3(−7)	4.0(−5)	6.5(−4)	4.4(−3)	2.1(−8)	8.1(−7)	1.2(−4)
^{208}Pb$(\overline{\nu_e},e^+)X$	1.1(0)	6.8(0)	2.3(1)	5.4(1)	4.7(−1)	1.9(0)	1.5(1)

nova neutrinos with high energetic Fermi-Dirac distributions follow a simple rule of thumb:

$$\sigma(\nu,\nu') = c(T,\alpha)A \times 10^{-42} \text{ cm}^2. \quad (4)$$

The proportionality factor depends on the parameters of the Fermi-Dirac spectrum. From RPA studies one finds $c(T,\alpha) \approx 0.7-0.9$ for $T=8$ MeV and $\alpha=0$ [45,22], while the proportionality factor is slightly smaller for closed-shell nuclei. We note that our present results fit well into the expected systematics: $c(T=8 \text{ MeV}, \alpha=0)=0.77$ for ^{56}Fe (open shell) and 0.67 for ^{208}Pb (closed shell).

Besides detecting a supernova neutrino signal, modern detectors should also have a ''neutrino spectroscopy ability''; i.e., it is desirable to assign observed events to the neutrino type which has triggered it. Detectors such as LAND and OMNIS will observe the neutrons produced by neutrino-induced reactions on ^{208}Pb. An obvious neutrino signal then is the total count rate. However, as already pointed out in [46], the total neutron count rate in a lead detector does not allow one to distinguish between events triggered by ν_e neutrinos and ν_x neutrinos. We confirm this argument as our total (ν_e,e^-n) cross section [e.g., for $(T,\alpha)=(4,0)$ it is 2.3×10^{-40} cm^2] is quite similar to the neutral-current cross section [for $(T,\alpha)=(8,0)$ neutrinos we find 1.4×10^{-40} cm^2 per neutrino family]. The situation is, however, different for ^{56}Fe. Here we find, for the same neutrino spectra as above, that the total neutron counting rate in the neutral-current reaction is about 30 times larger than for the charged-current reaction. If we consider that supernova ν_x neutrinos comprise four neutrino types with about the same spectrum, the neutron response of a ^{56}Fe detector to supernova neutrinos is expected to be dominated by neutral current events caused by ν_x neutrinos.

The differences in the ratios for neutral- and charged-current neutron yields again reflect the more general tendency that neutral-current cross sections for supernova ν_x neutrinos scale approximately with the mass number A of the target, while the charged-current cross sections for supernova ν_e neutrinos depend on the $N-Z$ neutron excess of the target via the Fermi and Ikeda sum rules (e.g., [22]). This suggests [46] that neutrino detectors which can only determine total neutron counting rates can have the supernova neutrino spectroscopy ability if they are made of various materials with quite different Z values as the ratio of neutral- to charged-current cross sections is quite sensitive to the charge number of the detector material. Of course, it is then necessary to assign observed events to the detector material.

Neutrino detectors of large size will probably not be built from isotopically enriched iron or lead, because the costs will be very high. Therefore, in principle, in addition to ^{56}Fe (91.75% natural abundance) and ^{208}Pb (52.4%), also cross sections for neutrino-induced reactions on the other stable isotopes ^{54}Fe (5.85%), ^{57}Fe (2.12%), ^{58}Fe (0.28%), ^{206}Pb (24.1%), ^{207}Pb (22.1%), and ^{204}Pb (1.4%) are needed. But from the rule of thumb [Eq. (4)] we can already conclude that the isotope effect on the neutral-current cross sections will be small. This has been confirmed for the iron isotope

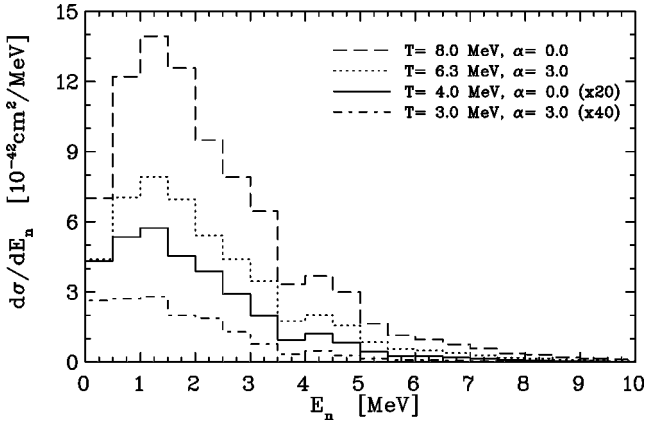

FIG. 4. Neutron energy spectrum produced by the charged-current (ν_e, e^-) reaction on ^{56}Fe. The calculation has been performed for different supernova neutrino spectra characterized by the parameters (T,α). Note that the cross sections for $(T,\alpha)=(4,0)$ and (3,3) neutrinos have been scaled by factors 20 and 40, respectively.

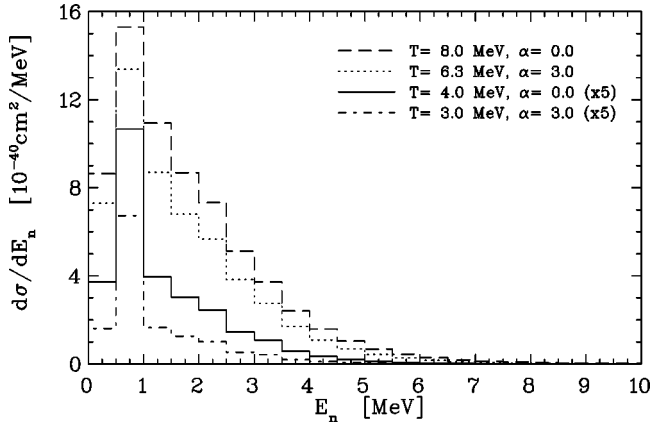

FIG. 6. Neutron energy spectrum produced by the charged-current (ν_e, e^-) reaction on ^{208}Pb. The calculation has been performed for different supernova neutrino spectra characterized by the parameters (T,α). Note that the cross sections for $(T,\alpha)=(4,0)$ and (3,3) neutrinos have been scaled by a factor of 5.

chain $^{52-58}$Fe within a recent shell model plus RPA approach which finds less than 16% deviation from the simple scaling rule [Eq. (4)] [48]. On the contrary the isotope effect on the charged-current cross sections will be strong, because they dominantly scale with $(N-Z)$ like mentioned above via the Fermi and Ikeda sum rules. This is again confirmed in the shell model plus RPA study which finds less than 10% deviation in the charged-current cross sections for $T=4$ MeV and $\alpha=0$ neutrinos from the simple $(N-Z)$ scaling [48]. We expect that the rule of thumb [Eq. (4)] and the $(N-Z)$ scaling is also valid for the neutral-current and charged-current reactions on ^{208}Pb, respectively. This provides then a simple scheme to estimate the charged-current cross sections for the other lead and iron isotopes.

Both the LAND and the OMNIS detectors will also be capable of detecting the neutron energy spectrum following the decay of states in the daughter nucleus after excitation by charged- and neutral-current neutrino reactions. We have calculated the relevant neutron energy spectra for both possible detector materials ^{56}Fe and ^{208}Pb. To this end we have used the statistical model code SMOKER iteratively by following the decay of the daughter states after the first particle decay. We have kept book of the neutron energies produced in these (sequential) decays and have binned them in 500-keV bins. The neutron energy spectra obtained this way are shown in Figs. 4–7. The calculations have been performed for different neutrino spectra which also allows one to study the potential sensitivity of the detectors if neutrino oscillations occur.

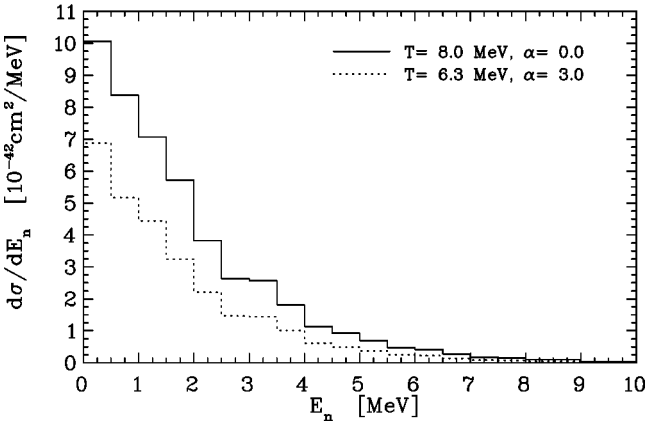

FIG. 5. Neutron energy spectrum produced by the neutral-current (ν,ν') reaction on ^{56}Fe. The calculation has been performed for different supernova neutrino spectra characterized by the parameters (T,α).

For the charged- and neutral-current reactions on ^{56}Fe the response is mainly below the $2n$ threshold. Most of the Gamow-Teller distribution is below the neutron threshold, as is the IAS in the charged-current reaction. The neutron energy spectrum of the ^{56}Fe$(\nu_e, e^- n)$ reaction is shown in Fig. 4.

The spectrum is rather structureless with a broad peak centered around neutron energies $E_n=1-1.5$ MeV and basically reflects the GT$_-$ distribution above the neutron threshold of 10.08 MeV. The respective neutron spectrum for the neutral current reaction is shown in Fig. 5.

The spectrum is composed by several (mainly first-forbidden) transitions which combined lead to a rather smooth neutron energy distribution. We note that the GT distribution is taken from the shell-model calculation and leads to a rather broad neutron spectrum.

The neutron spectrum for the charged-current reaction on ^{208}Pb is dominated by the Fermi transition to the IAS and by the GT$_-$ transitions. To understand the neutron spectrum we have to consider the neutron threshold energies for one-neutron decay (6.9 MeV) and for two-neutron decay (14.98 MeV) in ^{208}Bi. Hence the IAS and the collective GT resonance (with an excitation energy of about 16 MeV) will decay dominantly by $2n$ emission, while the low-lying GT$_-$ resonance at $E_x=7.6$ MeV decays by the emission of one neutron. This has significant consequences for the neutron spectrum. In two-neutron decay the available energy is shared between the two emitted particles, leading to a rather

broad and structureless neutron energy distribution. As can be seen in Fig. 6, this broad structure is overlaid with a peak at neutron energy around $E_n = 1$ MeV caused by the one-neutron decay of the lower GT$_-$ transition.

We expect that as a result of fragmentation, not properly described in our RPA calculation, the width of this peak might be broader than the 0.5 MeV binning which we have assumed in Fig. 6. We note that the relative height of the peak compared with the broad structure stemming from the $2n$ emission is more pronounced for the $(T,\alpha)=(4,0)$ neutrino distribution than for a potential $(T,\alpha)=(8,0)$ ν_e spectrum as it might arise after complete $\nu_e \leftrightarrow \nu_\mu$ oscillations.

Figure 7 shows the neutron energy spectrum for the neutral-current reactions on ^{208}Pb. Our RPA response places the strong GT transitions around the neutron threshold (at 7.37 MeV), while the first-forbidden transitions are split into several transitions between the excitation energies 9 MeV and 18 MeV. In particular, the two strong 1^- resonances at around 15 MeV and 18 MeV are above the two-neutron threshold at 14.12 MeV and their decay leads, for the same reasons as given above for the charged-current reaction, to a rather broad neutron energy spectrum. Several transitions above the one-neutron threshold superimpose in our RPA neutron spectrum this broad structure and lead to rather pronounced peaks. But nucleon-nucleon correlations beyond the RPA will induce a stronger fragmentation which will smear out these peaks. We expect therefore that the neutral-current neutron energy spectrum will be rather broad and structureless.

An exciting question is whether supernova neutrino detectors have the ability to detect neutrino oscillations. This can be achieved by a suited signal which allows one to distinguish between charged-current and neutral-current events and which is quite sensitive to the neutrino distribution. It is hoped that the detectors OMNIS and LAND have such an ability. However, as has been shown in [46], the total neutron counting rate is by itself not a suited mean to detect neutrino oscillations, even if results from various detectors with different material (hence different ratios of charged-to-neutral current cross sections, as discussed above) are combined. In Ref. [46] it is pointed out that in the case of ^{208}Pb an attractive signal might emerge. As a result of the fact that the IAS and large portions of the GT$_-$ strength resides in ^{208}Bi just above the two-neutron emission threshold, Fuller *et al.* discuss that the two-neutron emission rate is both flavor specific and very sensitive to the temperature of the ν_e distribution. To quantify this argument we have calculated the cross sections for the ^{208}Pb$(\nu_e,e^-2n)^{206}$Bi reaction in our combined model of the RPA for the neutrino-induced response and statistical model for the decay of the daughter states. We find partial cross sections of 43.9×10^{-42} cm^2 and 13.0×10^{-42} cm^2 for ν_e neutrinos with $(T,\alpha)=(4,0)$ and (3,3) Fermi-Dirac distributions. As pointed out in [46] these cross sections increase significantly if neutrino oscillations occur. For example, we find for total $\nu_e \leftrightarrow \nu_\mu$ oscillations partial $2n$ cross sections of 1053×10^{-42} cm^2 and 742×10^{-42} cm^2 [for neutrino distributions with parameters $(T,\alpha)=(8,0)$ and (6.26,3), respectively]. We remark that these numbers will probably be reduced if correlations beyond the RPA are taken into account as part of the GT$_-$ distribution might be shifted below the $2n$ threshold.

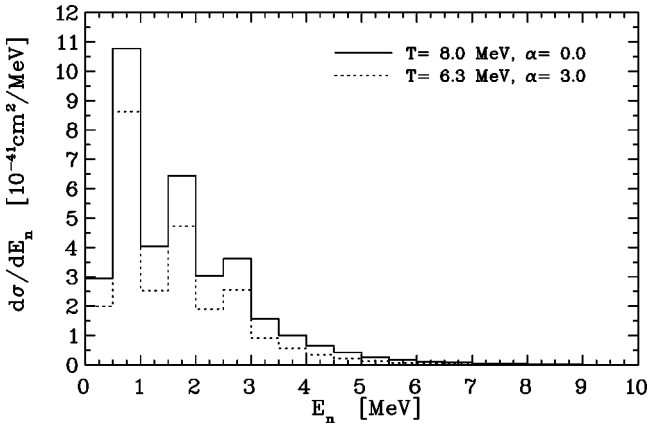

FIG. 7. Neutron energy spectrum produced by the neutral-current (ν,ν') reaction on ^{208}Pb. The calculation has been performed for different supernova neutrino spectra characterized by the parameters (T,α).

As pointed out above, also portions of the neutral-current excitation spectrum are above the respective $2n$-emission threshold. This decay will compete with the one stemming from the charged-current reaction and hence will reduce the flavor sensitivity of the signal. We have therefore also calculated the ^{208}Pb$(\nu,\nu'2n)^{206}$Pb cross sections and find 41.3×10^{-42} cm^2 and 23.5×10^{-42} cm^2 [for neutrino distributions with $(T,\alpha)=(8,0)$ and (6.26,3), respectively and averaged over neutrinos and antineutrinos]. Thus, if no neutrino oscillations occur, the combined $2n$ signal resulting from neutral-current reactions for the four ν_x neutrino types is larger than the one from the charged-current reactions. However, if neutrino oscillations occur, the neutral-current signal is unaffected while the charged-current signal is drastically enhanced. Thus, our calculations support the suggestions of Ref. [46] that the $2n$ signal for ^{208}Pb detectors might be an interesting neutrino oscillation signal. However, our calculations also indicate that, for an analysis of the potential observation of the signal, two-neutron emission from neutral-current events has to be accounted for as well.

Finally, as the predicted energy spectra of neutrinos from supernovas change with time and furthermore can be affected in a variety of ways (especially oscillation scenarios), Table VI lists the cross sections for (ν_e,e^-) and (ν,ν') scattering on ^{56}Fe and ^{208}Pb as a function of neutrino energy.

IV. CONCLUSIONS

We have studied the charged- and neutral-current reactions on ^{56}Fe and ^{208}Pb which are the shielding materials for current accelerator-based neutrino experiments such as LSND and KARMEN and the material for proposed supernova neutrino detectors such as LAND and OMNIS.

Our calculations for ^{56}Fe are performed within a model which uses the interacting shell model to determine the Gamow-Teller response and the RPA for forbidden transitions. For ^{208}Pb the complete nuclear response is evaluated

TABLE VI. Total ^{56}Fe$(\nu_e,e^-)X$, ^{56}Fe$(\nu,\nu')X$, ^{208}Pb$(\nu_e,e^-)X$, and ^{208}Pb$(\nu,\nu')X$ cross sections for selected neutrino energies E_ν. The cross sections are given in 10^{-42} cm^2, while the energies are in MeV. Exponents are given in parentheses.

E_ν	^{56}Fe$(\nu_e,e^-)X$	^{56}Fe$(\nu,\nu')X$	^{208}Pb$(\nu_e,e^-)X$	^{208}Pb$(\nu,\nu')X$
10	6.61 (−1)	1.91 (−1)	9.34 (0)	7.14 (−1)
15	6.45 (0)	2.19 (0)	1.41 (+2)	7.98 (0)
20	2.93 (+1)	6.90 (0)	4.85 (+2)	2.54 (+1)
25	7.33 (+1)	1.51 (+1)	1.32 (+3)	5.84 (+1)
30	1.40 (+2)	2.85 (+1)	2.48 (+3)	1.14 (+2)
35	2.36 (+2)	4.89 (+1)	3.99 (+3)	1.99 (+2)
40	3.71 (+2)	7.86 (+1)	5.72 (+3)	3.17 (+2)
45	5.55 (+2)	1.19 (+2)	7.63 (+3)	4.72 (+2)
50	7.98 (+2)	1.72 (+2)	9.69 (+3)	6.65 (+2)
55	1.10 (+3)	2.39 (+2)	1.20 (+4)	8.96 (+2)
60	1.48 (+3)	3.20 (+2)	1.45 (+4)	1.17 (+3)
65	1.92 (+3)	4.15 (+2)	1.73 (+4)	1.48 (+3)
70	2.42 (+3)	5.25 (+2)	2.02 (+4)	1.83 (+3)
75	2.99 (+3)	6.50 (+2)	2.31 (+4)	2.22 (+3)
80	3.60 (+3)	7.89 (+2)	2.62 (+4)	2.65 (+3)
85	4.27 (+3)	9.42 (+2)	2.93 (+4)	3.11 (+3)
90	4.98 (+3)	1.11 (+3)	3.26 (+4)	3.61 (+3)
95	5.73 (+3)	1.29 (+3)	3.60 (+4)	4.13 (+3)
100	6.52 (+3)	1.49 (+3)	3.96 (+4)	4.69 (+3)
105	7.36 (+3)	1.70 (+3)	4.33 (+4)	5.26 (+3)
110	8.24 (+3)	1.92 (+3)	4.71 (+4)	5.86 (+3)
115	9.16 (+3)	2.16 (+3)	5.10 (+4)	6.47 (+3)
120	1.01 (+4)	2.41 (+3)	5.50 (+4)	7.09 (+3)
125	1.11 (+4)	2.66 (+3)	5.90 (+4)	7.73 (+3)
130	1.21 (+4)	2.92 (+3)	6.31 (+4)	8.37 (+3)
135	1.32 (+4)	3.19 (+3)	6.71 (+4)	9.01 (+3)
140	1.42 (+4)	3.46 (+3)	7.12 (+4)	9.66 (+3)
145	1.53 (+4)	3.74 (+3)	7.52 (+4)	1.03 (+4)
150	1.64 (+4)	4.01 (+3)	7.91 (+4)	1.09 (+4)

within the RPA model. The correct momentum dependence of the various multipole operators is considered. This leads to a reduction of the cross sections, compared to calculations performed at $q=0$, due to destructive interference with ''higher-order'' multipole operators.

At first we have calculated the total cross sections and the partial cross sections for spallating a neutron from the target for muon-decay-at-rest neutrinos. Additionally we have evaluated the charged-current cross section on ^{208}Pb as a function of final lepton energy. All these quantities are expected to allow for (even) more reliable background simulations for the LSND and KARMEN detectors. As the LSND Collaboration might have observed a neutrino-oscillation signal we have also calculated the various cross sections on ^{56}Fe and ^{208}Pb for pion-in-flight-decay neutrinos as they comprise a small admixture of ν_μ neutrinos in the LSND beam.

Detecting supernova neutrinos is generally considered an important test of theoretical models for core-collapse supernovas. OMNIS and LAND are two proposed detectors, consisting of lead and possibly iron, which will have the capability to count the total rate of neutrons produced by neutrino reactions in the detector and further to detect the related neutron energy spectrum. For ^{56}Fe the decay is mainly by emission of one neutron. Nevertheless, the neutron energy spectrum is rather broad and structureless following both charged- and neutral-current excitations.

For ^{208}Pb the situation is different as a significant portion of the charged-current response (and also of the neutral-current response) is above the $2n$ threshold. As the two neutrons share the available decay energy this leads to a rather broad neutron spectrum. For the charged-current reaction we predict that this broad pattern is superimposed by a peak structure, due to a yet unobserved Gamow-Teller transition at lower energies. We find that the height of this peak relative to the broad structure is more pronounced for ''ordinary'' ν_e supernova neutrinos than for a ν_e neutrino spectrum arising after $\nu_\mu \to \nu_e$ oscillations. Another possible oscillation signal for a ^{208}Pb detector is the emission rate of two neutrons, as suggested by Fuller, Haxton, and McLaughlin. We have quantitatively confirmed the argument of these authors and have also calculated the two-neutron emission rate for the neutral-current reaction which has to be considered if, in the event of a nearby supernova, the two-neutron emission signal would be observed and analyzed for oscillation information.

ACKNOWLEDGMENTS

We thank G. Drexlin and M. Steidl from the KARMEN Group for stimulating and helpful discussions. We are also grateful to G. Martínez-Pinedo for his help with the shell-model calculations. The work has been partly supported by a grant of the Danish Research Council.

[1] G. Raffelt, *Stars as Laboratories for Fundamental Physics* (University of Chicago Press, Chicago, 1996).
[2] LSND Collaboration, C. Athanassopoulos *et al.*, Phys. Rev. C **54**, 2685 (1996); Phys. Rev. Lett. **77**, 3082 (1996); **81**, 1774 (1998).
[3] J.N. Bahcall, *Neutrino Astrophysics* (Cambridge University Press, Cambridge, England, 1989).
[4] Y. Fukuda *et al.*, Phys. Rev. Lett. **81**, 1562 (1998).
[5] T. Stanev, Nucl. Phys. **B48**, 165 (1996).
[6] MINOS Collaboration, P. Adamson *et al.*, MINOS Detectors Technical Design Report No. NuMI-L-337, 1998.
[7] KARMEN Collaboration, B. Armbruster *et al.*, Phys. Rev. C **57**, 3414 (1998), and references therein.
[8] K. Hirata *et al.*, Phys. Rev. Lett. **58**, 1490 (1987).
[9] R.M. Bionta *et al.*, Phys. Rev. Lett. **58**, 1494 (1987).
[10] P.F. Smith, Astropart. Phys. **8**, 27 (1997); in *Proceedings of the 3rd International Conference on Sources of Dark Matter*, Marina del Rey (Elsevier, New York, 1998), p. 465; in *Proceedings of the 4th International Conference on Sources of Dark Matter*, Marina del Rey, 2000 (Springer, New York, in

press).
[11] D.B. Cline *et al.*, Astrophys. Lett. Commun. **27**, 403 (1990); Phys. Rev. D **50**, 720 (1994).
[12] C.K. Hargrove *et al.*, Astropart. Phys. **5**, 183 (1996).
[13] G. Ewan, Nucl. Instrum. Methods Phys. Res. A **314**, 373 (1992); SNO Collaboration, Phys. Can. **48**, 112 (1992).
[14] K. Langanke, P. Vogel, and E. Kolbe, Phys. Rev. Lett. **76**, 2629 (1996).
[15] R. Maschuw, Prog. Part. Nucl. Phys. **40**, 183 (1998); K. Eitel (private communication).
[16] E. Kolbe, K. Langanke, and G. Martínez-Pinedo, Phys. Rev. C **60**, 052801 (1999).
[17] J.D. Walecka, in *Muon Physics*, edited by V.W. Hughes and C.S. Wu (Academic, New York, 1975), Vol. II, p. 113.
[18] E. Caurier, K. Langanke, G. Martínez-Pinedo, and F. Nowacki, Nucl. Phys. **A653**, 439 (1999).
[19] B.A. Brown and B.H. Wildenthal, Annu. Rev. Nucl. Part. Sci. **38**, 29 (1988).
[20] K. Langanke, D.J. Dean, P.B. Radha, Y. Alhassid, and S.E. Koonin, Phys. Rev. C **52**, 718 (1995).
[21] G. Martínez-Pinedo, A. Poves, E. Caurier, and A.P. Zuker, Phys. Rev. C **53**, R2602 (1996).
[22] A. Hektor, E. Kolbe, K. Langanke, and J. Toivanen, Phys. Rev. C **61**, 055803 (2000).
[23] G.A. Rinker and J. Speth, Nucl. Phys. **A306**, 360 (1978).
[24] M.R. Plumley *et al.*, Phys. Rev. C **56**, 263 (1997).
[25] E. Kolbe, K. Langanke, S. Krewald, and F.K. Thielemann, Nucl. Phys. **A540**, 599 (1992).
[26] E. Kolbe, K. Langanke, and P. Vogel, Nucl. Phys. **A652**, 91 (1999).
[27] E. Kolbe, K. Langanke, and S. Krewald, Phys. Rev. C **49**, 1122 (1994).
[28] E. Kolbe, K. Langanke, F.-K. Thielemann, and P. Vogel, Phys. Rev. C **52**, 3437 (1995).
[29] E. Kolbe, K. Langanke, and P. Vogel, Phys. Rev. C **50**, 2576 (1994).
[30] E. Kolbe, K. Langanke, and P. Vogel, Nucl. Phys. **A613**, 382 (1996).
[31] J.J. Cowan, F.-K. Thielemann, and J.W. Truran, Phys. Rep. **208**, 267 (1991).
[32] D.J. Horen *et al.*, Phys. Lett. **95B**, 27 (1981).
[33] C. Gaarde *et al.*, Nucl. Phys. **A369**, 258 (1981).
[34] H. Sagawa and N. Van Giai, Phys. Lett. **113B**, 119 (1982).
[35] T. Suzuki, D.F. Measday, and J.P. Roalsvig, Phys. Rev. C **35**, 2212 (1987).
[36] E. Kolbe, K. Langanke, and P. Vogel, Phys. Rev. C **62**, 055502 (2000).
[37] LSND Collaboration, C. Athanassopoulos *et al.*, Nucl. Instrum. Methods Phys. Res. A **388**, 149 (1997).
[38] LSND Collaboration, C. Athanassopoulos *et al.*, Phys. Rev. C **56**, 2806 (1997).
[39] LSND Collaboration, C. Athanassopoulos *et al.*, Phys. Rev. C **58**, 2489 (1998).
[40] H.-T. Janka and W. Hillebrandt, Astron. Astrophys. **224**, 49 (1989); Astron. Astrophys., Suppl. Ser. **78**, 375 (1989).
[41] J.R. Wilson (private communication), as cited in [45].
[42] G.E. Brown and J. Speth, Nucl. Phys. **A330**, 294 (1979).
[43] A. Veyssiere *et al.*, Nucl. Phys. **A159**, 561 (1970).
[44] T. Suzuki, invited talk at the International Conference on ''Giant Resonances,'' Osaka, Japan, 2000.
[45] Y.-Z. Qian, W.C. Haxton, K. Langanke, and P. Vogel, Phys. Rev. C **55**, 1532 (1997).
[46] G.M. Fuller, W.C. Haxton, and G.C. McLaughlin, Phys. Rev. D **59**, 085005 (1999).
[47] S.E. Woosley, D.H. Hartmann, R.D. Hoffman, and W.C. Haxton, Astrophys. J. **356**, 272 (1990).
[48] J. Toivanen, E. Kolbe, K. Langanke, G. Martinez-Pinedo, and P. Vogel, Nucl. Phys. A (submitted).